may indicate that conifers preferred seasonally dry soils more prone to forest fire than is likely for the Farnberg paleosol.

Thick cross-bedded sandstone interbedded with the Farnberg paleosol (Fig. 3) is a paleochannel and indicates a connected drainage through this upper portion of the partly filled paleokarst. The Farnberg paleosol formed on well-drained valley slopes of this polje between hills of karst and chert of the Ozark highlands to the south and extensive seas and swamps of lowlands to the north (*9*). Parent material of the Farnberg paleosol included flint clays remaining from paleokarst dissolution, slope wash, and a small amount of fresh fluvial deposits and air-fall dust. Relict bedding can be discerned in the basal part of the profile, but none remains in the rooted horizons (Fig. 2). By comparison with modern soils (*35*), this observation indicates at least tens of thousands of years of soil formation. Soil formation could have extended for millions of years to create such deeply weathered material, but it is likely that a substantial component of this chemical weathering occurred in preexisting soils that were eroded to provide the parent material of the Farnberg paleosol (*9*).

Fossil trees and forested paleosols are known to be as ancient as the Middle Devonian (*22*), but none of these Devonian paleosols are nearly as base-depleted as the Farnberg paleosol. Quartz sandstones with large fossil root traces represent other kinds of oligotrophic soils (Spodosols, Dystrochrepts, and Quartzipsamments) and, like the Farnberg paleosol, are also no older than the Carboniferous (*22, 36*). No Devonian or older orthoquartzites or bauxites are known to contain large woody root traces. These are difficult substrates for plants, and the coevolution of nutrient-conserving ecosystems capable of sustained growth on such soils may have taken some time. Whether it took as long as the Late Devonian and Mississippian for trees to adapt to such infertile soils remains to be seen from the continuing search for fossil root traces and paleosols.

REFERENCES AND NOTES

1. G. J. Retallack, *Paleobiology* **59**, 59 (1984).
2. G. Krumbiegel, L. Rüffle, H. Haubold, *Das Eozäne Geiseltal* (Ziemsen, Lutherstadt, Germany, 1983); M. Archer, S. J. Hand, H. Godthelp, *Riversleigh* (Reed, Sydney, 1991).
3. J. A. Wolfe, *Geophys. Mon. Am. Geophys. Union* **12**, 357 (1985).
4. G. W. Rothwell, *Paleontographica* **B151**, 171 (1975).
5. W. A. DiMichele and T. L. Phillips, *Rev. Palaeobot. Palynol.* **27**, 103 (1979).
6. V. A. Krassilov, *Paleoecology of Terrestrial Plants* (Wiley, New York, 1975).
7. R. L. Sanford, *Science* **235**, 1062 (1987).
8. The Farnberg pit is 200 m east of the Bueker pit in the NE1/4, NW1/4, SW1/4 section 30 T43N R5W, Gasconade County. The Farnberg clay paleosol is in the upper level of the southern side of the pit and was measured and collected on 3 November 1989.
9. W. D. Keller, J. F. Westcott, A. O. Bledsoe, in *Clays and Clay Minerals*, A. Swineford and N. Plummer, Eds. (National Academy of Sciences, Washington, DC, 1954), pp. 7–46.
10. D. E. Zeller, Ed., *Bull. Kans. Geol. Surv.* **189** (1968); H. B. Willman *et al.*, *Bull. Ill. Geol. Surv.* **95**, 1 (1975).
11. W. B. Harland *et al.*, *A Geologic Time Scale 1989* (Cambridge Univ. Press, Cambridge, 1990).
12. J. Walton, *Philos. Trans. R. Soc. London Ser. B* **226**, 219 (1936).
13. G. J. Retallack, *Annu. Rev. Earth Planet. Sci.* **19**, 183 (1991).
14. C. Beaumont, G. Quinlan, J. Hamilton, *Tectonics* **7**, 389 (1988).
15. H. H. Damberger, *Econ. Geol.* **66**, 488 (1971); C. E. Robertson, *Rep. Invest. Mo. Geol. Surv. Water Res.* **54**, 1 (1973).
16. A. G. Epstein, J. B. Epstein, C. D. Harris, *U.S. Geol. Surv. Prof. Pap.* **995**, 1 (1977); A. G. Harris, C. B. Rexroad, R. T. Lierman, R. A. Askin, *Cour. Forsch. Inst. Senckenberg* **118**, 253 (1990).
17. Compaction (C) as a fraction can be calculated from depth (D) in kilometers from
$$C = -0.5/\{[0.49/e^{(D/3\ 7)}]-1\}$$
from J. G. Sclater and P. A. F. Christie [*J. Geophys. Res.* **85**, 3711 (1980)].
18. Y. Lucas, F. J. Luizão, A. Chauvel, J. Rouiller, D. Nahon, *Science* **260**, 521 (1993).
19. H. A. Tourtelot, M. B. Goldhaber, M. R. Hudson, *Geol. Soc. Am. Abstr. Prog.* **20**, A140 (1988).
20. D. L. Leach and E. L. Rowan, *Geology* **14**, 931 (1986).
21. A. V. Heyl, in *International Conference on Mississippi Valley–Type Lead-Zinc Deposits*, G. Kisvarsanyi, S. K. Grant, W. P. Pratt, J. W. Koenig, Eds. (Univ. of Missouri Press, Rolla, MO, 1983), pp. 27–60; C. Bethke, *Econ. Geol.* **81**, 233 (1986).
22. J. C. Brannon, F. A. Podosek, R. K. McLimans, *Nature* **356**, 509 (1992).
23. G. J. Retallack, *Soils of the Past* (Unwin-Hyman, London, 1990).
24. J. Karweil, in *Petrographie Organique et Potential Petrolier*, B. Alpern, Ed. (Centre National du Recherche Scientifique, Paris, 1975), pp. 195–203.
25. P. A. Sanchez, *Properties and Management of Soils in the Tropics* (Wiley, New York, 1976).
26. Soil Survey Staff, *Keys to Soil Taxonomy* (Tech. Monogr. 19, Soil Management Support Services, Blacksburg, VA, 1990).
27. Food and Agriculture Organization, *UNESCO Soil Map of the World* (1971–1981).
28. G. J. Retallack, *Miocene Paleosols and Ape Habitats in Pakistan and Kenya* (Oxford Univ. Press, New York, 1991).
29. G. D. Sherman, in *Problems of Clay and Laterite Genesis*, A. F. Frederickson, Ed. (American Institute of Mining and Metallurgical Engineering, New York, 1952), pp. 154–161; C. E. Weaver, *Clays, Muds and Shales* (Elsevier, Amsterdam, 1989).
30. W. A. DiMichele and R. W. Hook, in *Terrestrial Ecosystems Through Time*, A. K. Behrensmeyer, J. D. Damuth, W. A. DiMichele, R. Potts, H.-D. Sues, S. L. Wing, Eds. (Univ. of Chicago Press, Chicago, 1992), pp. 205–323.
31. R. L. Leary, *Rep. Invest. Ill. State Mus.* **37**, 1 (1981); *Science* **249**, 1152 (1990).
32. S. H. Mamay, *Am. J. Bot.* **76**, 1299 (1989); G. J. Retallack, field observations.
33. D. White, *Carnegie Inst. Washington Publ. 405*, (1929), p. 1; G. J. Retallack, field observations.
34. A. C. Scott and W. G. Chaloner, *Proc. R. Soc. London Ser. B* **220**, 163 (1983).
35. P. W. Birkeland, *Geomorphology* **3**, 207 (1990).
36. S. D. Vanstone, *J. Sediment. Petrol.* **61**, 445 (1991).
37. Chemical analyses were done by C. McBirney using atomic adsorption, with errors from 10 replicate analyses of standard rock (W2).
38. Thermal analysis by M. Földvári and J. Germán-Heins.

31 January 1994; accepted 23 May 1994

Fabrication of Atomic-Scale Structures on Si(001) Surfaces

C. T. Salling and M. G. Lagally*

The scanning tunneling microscope has been used to define regular crystalline structures at room temperature by removing atoms from the silicon (001) surface. A single atomic layer can be removed to define features one atom deep and create trenches with ordered floors. Segments of individual dimer rows can be removed to create structures with atomically straight edges and with lateral features as small as one dimer wide. Conditions under which such removal is possible are defined, and a mechanism is proposed.

The ability of the scanning tunneling microscope (STM) to fabricate ordered atomic-scale structures of any desired geometry (*1–3*) and to probe their properties opens new frontiers for investigation, including studies of spatially resolved electron interference in model systems (*4*) and current modulation mechanisms for electronic devices with atomic-scale active areas (*5*). The four main categories of fabrication with the STM are (i) arranging adatoms into a pattern (*1, 4*), (ii) writing patterns by depositing atoms onto the surface from the tip (*6, 7*) or by decomposing precursor molecules (*8, 9*), (iii) using the STM to create an etch mask (*10, 11*), and (iv) defining patterns by transferring unwanted atoms from the surface to the tip (*2, 3*). For the investigation of nanoelectronic devices and model systems, an important aspect of any of these fabrication methods is the ability to produce atomically ordered structures of any desired geometry. Removing material from an already well-ordered surface is the most straightforward method for creating crystalline atomic-scale structures with well-defined and regular features that are stable at ordinary temperatures.

Materials Science and Engineering Department, University of Wisconsin-Madison, Madison, WI 53706, USA.

*To whom correspondence should be addressed.

Atomic-scale fabrication by removal is based on the ability of the STM to transfer unwanted atoms from a sample's surface to the STM tip (*2, 3, 12–14*). The removal process is similar to field evaporation (*13*) but can involve the formation of a bridge of atoms between the tip and sample (*12*). Regular structures with lateral dimensions as small as a single atom have been fabricated with the STM by the removal of individual atoms in rows from the sulfur-terminated surface of cleaved MoS_2 (*2*). Similarly, rough-edged structures as narrow as ~30 Å have been defined (*3*) by the formation of trenches on the (7×7) reconstructed Si(111) surface. The floors of trenches and pits formed on Si(111) either were not imaged (*12*) or were shown to be disordered (*13*).

We have been able to fabricate on the Si(001) surface atomic-scale structures that have atomically straight edges and to create pits and trenches that have ordered floors. Our ability to do so rests on the anisotropy of the Si(001) surface structure and the careful adjustment of the conditions for atom removal. We demonstrate here the types of patterns that can be formed and describe the conditions required to achieve them.

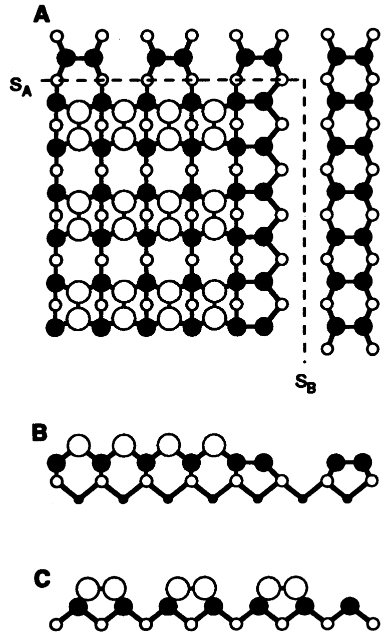

Fig. 1. Diagram of a vicinal Si(001) surface. (**A**) Plan view, showing three atomic layers. The largest circles represent atoms in the top layer; midsize and small circles represent atoms in the next two layers, respectively. The atoms in the top layer form rows of dimers, which appear as light stripes in the STM images. The distance between adjacent dimers in a row is 3.85 Å, and the spacing between adjacent dimer rows is 7.7 Å. (**B**) Cross-sectional view in a plane parallel to the dimer row direction. (**C**) Cross-sectional view in a plane perpendicular to the dimer row direction.

The experiments were conducted with an STM in ultrahigh vacuum with STM tips prepared from polycrystalline tungsten wire. A clean, sharp tip is required to achieve the fabrication results reported here. The Si(001) samples were cut from [001] *p*-type silicon wafers having a resistivity of 10 ohm·cm and were cleaned in situ by a standard procedure (*15*). The atoms of the Si(001) surface are laterally bonded into rows of dimers and form a (2×1) reconstruction (Fig. 1). Vicinal Si(001) surfaces consist of terraces separated by monatomic steps. Because silicon has the diamond crystal structure, the orientation of the dimer rows alternates between two perpendicular directions from one terrace to the next. For a particular direction of miscut (toward the [110] direction), the steps are alternately rough, when the dimer rows on the upper terrace are perpendicular to the step (called an S_B step), and smooth, when the dimer rows on the upper terrace are parallel to the step (called an S_A step). This step morphology reflects the bonding anisotropy of the atoms in the Si(001) surface: Once dimers have formed, the sides of the dimer rows are unreactive, whereas the ends of rows are much more reactive.

To image the Si(001) surface, we set the feedback circuit of the STM to maintain a constant tunneling current of 0.2 nA at a tip voltage of +2 V with respect to the sample. This condition corresponds to a tip-sample separation s_0 during imaging. To remove atoms from the sample surface, the feedback circuit is disengaged, the tip is displaced (with 0 V on the tip) toward the sample by a known amount to give a tip-sample separation $s < s_0$, and the tip voltage is pulsed to a selected value for 10 ms. The tip is then retracted with 0 V on the tip, the tip voltage is returned to +2 V, the feedback circuit is engaged, and imaging is commenced. As the pulse voltage is increased in a series of removal attempts (at fixed *s*), the probability *P* for transferring material from the surface to the tip increases from 0 to 1 over a voltage range of ~0.2 V. We define the threshold voltage as the median of this voltage range. We determine the threshold voltage by increasing the pulse voltage in increments of 0.1 to 0.2 V until a series of six attempts results in the removal of atoms with $P \approx 0.5$. For experiments at $s = 1.5$ Å, the measured value of -3.6 ± 0.2 V for the threshold voltage allows us to estimate an upper limit of 2 V/Å for the threshold field for atom removal on Si(001).

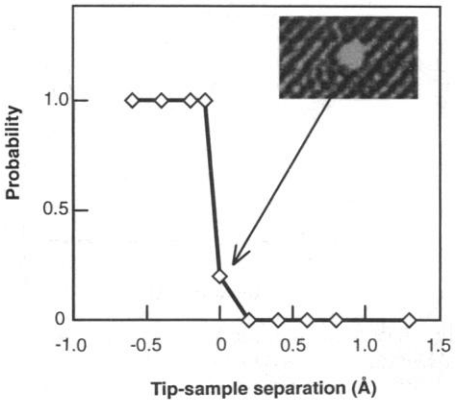

Fig. 2. The probability of creating a hillock as a function of tip-sample separation, *s*, for a sequence of tip displacements toward the sample with 0 V on the tip. The point at which there is a measurable probability of mechanical contact is defined as the point of zero tip-sample separation. The tip position during imaging is found to be 5.8 Å with respect to the mechanical contact point. (**Inset**) An STM image (87 Å by 54 Å) of a typical hillock resulting from mechanical contact.

The threshold voltage necessary to remove atoms depends on *s*, which is the difference between s_0 and the displacement of the tip from s_0 before the removal attempt. To obtain a value for s_0, a fiducial point must be established. As the tip is displaced toward the surface with 0 V on the tip, a hillock is formed on the surface when the displacement is large enough (Fig. 2). We have defined the point at which the probability of forming a hillock is 0.2 as "mechanical contact" and have chosen it as the zero point for measuring the tip-sample separation. The value of s_0 is therefore the difference between the tip position during the imaging condition described above and the position at mechanical contact. The value of s_0 depends on the apex morphology of the tip. Hence, s_0 must be measured for each new tip. Because atom removal can change the apex morphology, s_0 must be periodically remeasured during a sequence of removal events. Values of s_0 fall in the range 6.6 Å > s_0 > 4.8 Å for all tips that yield good images at a tunneling current of 0.2 nA and a tip bias of +2 V. For a given tip, the measured variation in s_0 is ±0.1 Å during imaging and ±0.3 Å during a sequence of removal events. In the present experiments, the uncertainty in *s* of ±0.3 Å reflects the fact that s_0 was remeasured only periodically and not after every removal event.

Three types of surface modification can result from a voltage pulse. An incomplete transfer of material to the tip results in the formation of hillocks (Fig. 2, inset) and hillocks surrounded by moats. The complete transfer of material to the tip results in the formation of a pit. These three types of structures were also observed in previous work on Si(111) (*11*). As the voltage pulse height is increased during a series of removal events, we find that the most probable outcome is a hillock for low voltages, a hillock surrounded by a moat for higher voltages, and a pit for voltages at or above the threshold value.

The results of removing the top layer of atoms from a region of the Si(001) surface by the application of a single threshold voltage pulse at $s = 1.5$ Å are shown in Fig. 3. The tip was positioned over the desired location by iteration: We manually adjusted the tip's position and monitored it by using single STM scans along lines that include "landmarks" such as steps or fabricated structures. Approximately 24 atoms were removed by the pulse to create the rectangular pit shown in Fig. 3A. Its shape is typical of pits on Si(001): square or rectangular and bounded by edges that correspond to S_A and S_B steps. The newly exposed layer of atoms has the (2×1) reconstruction of Si(001). An STM scan (Fig. 3B) shows that a single atomic layer has been removed, because the depth of the pit is equal to the height of a monatomic step ($\sim$1.4 Å).

The importance of the threshold voltage in the atom removal process is illustrated in Fig. 4A, which shows two trenches that were fabricated by the creation of a series of adjacent pits. For both trenches, the initial pit was created at $s = 1.5$ Å. As trench 1 was formed, the pulse voltage was readjusted after each successful removal to remain at threshold. This readjustment is required to compensate for the ±0.3 Å changes in s_0 mentioned above that are caused by changes in tip morphology during atom removal. On the other hand, trench 2 was formed at a constant voltage that was above threshold ($P = 1$). The floor of trench 1 has a nearly perfect (2×1) structure, whereas the floor of trench 2 is disordered with an uneven depth. Scans with the STM across the trenches confirm that trench 1 is a single atomic layer deep (Fig. 4B), whereas trench 2 has a depth of up to three atomic layers (Fig. 4C).

Segments can be removed repeatedly as single events from an individual dimer row of the Si(001) surface without disturbing the atoms in neighboring rows to define structures with atomically straight edges. In Fig. 5A, pit 1 is two dimer rows wide and was fabricated at $s = 1.5$ Å, like the pit in Fig. 3. Pit 2 is one dimer row wide and was created at $s = 1.1$ Å, which was also used for all subsequent removal events in Fig. 5. We attribute the improved resolution for fabrication during and after the creation of pit 2 to the smaller tip-sample separation and the possibility that the nanotip (composed of silicon) had become sharper. Starting at pit 2, segments two to three dimers long were removed from an individual dimer row to create the trench ($\sim$12 Å wide) shown in Fig. 5B. Similarly, the upper trench in Fig. 5C was formed starting from pit 1. Next, the top layer of atoms was removed from the regions at the ends of the ridge in Fig. 5C to create the isolated island structure shown in Fig. 5D. The "moat" that defines the island is one atomic layer deep and has a well-ordered floor exhibiting the (2×1) reconstruction of Si(001).

In the sequence of events presented in Fig. 6, sections of dimer rows three to six dimers (11.5 to 23 Å) long were removed from the edges of initially rough trenches to define a ridge three dimer rows (23 Å) wide that has atomically straight edges. During the fabrication sequence, a total of 21 dimers were removed from the edges of the two trenches, yet only one defect was introduced in a neighboring row (indicated by the arrow in Fig. 6B, at the far end of a removed segment). This high selectivity allows a high success rate for creating perfect or nearly perfect ridges, islands, or peninsulas with rectangular shapes.

The ability to remove dimer row segments from the edges of S_A steps without disturbing the dimers in neighboring rows demonstrates that it is easier to remove dimers along a dimer row than perpendicular to it (at least when using threshold voltages for $s = 1$ to 1.5 Å). This trend parallels the stability of the steps: S_A is very stable and chemically unreactive, whereas S_B is the opposite (*16*). The reason for this difference in stability is that no unsaturated electronic charge is available at the sides of

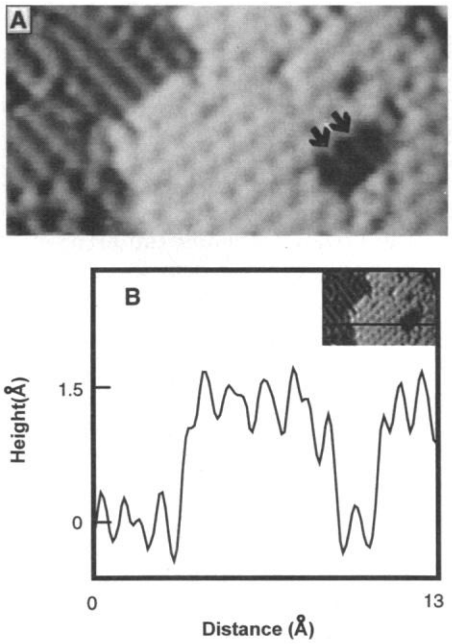

Fig. 3. Removal of a single atomic layer. (**A**) An STM image (140 Å by 70 Å) of a rectangular pit (two dimer rows wide and six dimers long) that was formed by the removal of a single layer of atoms from the upper-terrace region. The arrows indicate the positions of the dimer rows in the second atomic layer, which forms the floor of the pit. (**B**) Linescan across the pit and neighboring step, along the line indicated in the inset. The corrugation in the sample height on the upper terrace, lower terrace, and pit floor is caused by scanning across the surface's dimer rows. The change in the average value shows that the depth of the pit is equal to the height of the step.

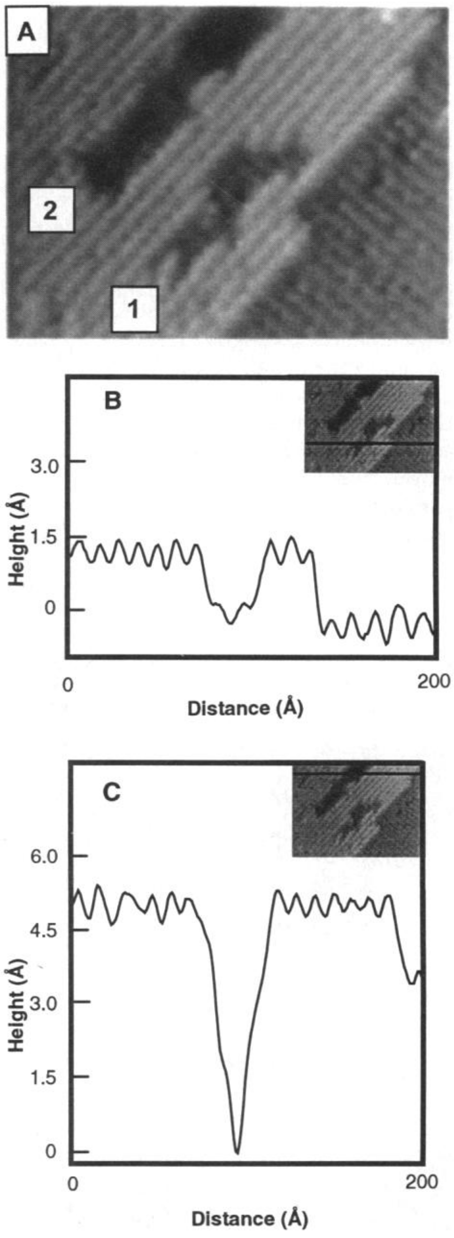

Fig. 4. Two trenches made from overlapping pits, illustrating the importance of not exceeding the threshold condition in order to create regions one atomic layer deep that have ordered floors. (**A**) An STM image (200 Å by 200 Å) of the trenches. Trench 1 was made with pulses of −3.5 to −3.7 V at $s = 1.8$ Å, which were at threshold. Trench 2 was made with −3.7-V pulses at $s = 1.6$ Å, which were above threshold. (**B**) An STM scan across trench 1 along the line indicated in the inset. (**C**) An STM scan across trench 2 along the line indicated in the inset.

a dimer row; at the ends of the rows, bonds are available. This anisotropy also manifests itself in the growth shape of silicon islands, which are long strings with S_A sides and S_B ends.

The mechanism of the removal process may be viewed microscopically as follows. In earlier work on Si(111) (*12*), the current was monitored during the removal attempt and was found to exhibit hysteresis when a hillock-and-moat combination was formed. It was suggested that this hysteresis indicates that the removal of atoms (at least for small values of *s*) is a two-stage process. When a sufficiently large voltage pulse is applied, the tip and sample atoms displace toward each other enough to form a bridge between the tip and sample. This bridge breaks during the voltage pulse or during the retraction of the tip. The type of surface modification (hillock, hillock and moat, or pit) depends on where the bridge breaks. Applying the same argument here, we find that the threshold voltage is the minimum voltage that results in the bridge breaking at its base, in the sample. When threshold voltage pulses are used, the bonds that break are between the atoms in the top and second layers.

The fact that using the minimum pulse voltage allows us to remove only the atoms in the top layer suggests that the field induced by the tip falls off rapidly as it penetrates the crystal, with the result that the perturbation of the bonds between the second and third layers of atoms is insufficient to remove atoms in the second layer. Similarly, the fact that it is easier to remove atoms along a row rather than perpendicular to it reflects the anisotropy in the bonding of the reconstructed surface layer of atoms to the second-layer atoms (Fig. 1). When a dimer in a given row on the surface is displaced toward the tip, it pulls up on the four atoms in the second layer to which it is connected (Fig. 1B). Displacing these second-layer atoms weakens their bonds to the surface dimers directly on either side of the one being displaced. This strain does not, however, affect the bonding of dimers in neighboring rows except through the third layer, as can be seen in Fig. 1C. The silicon crystal structure and the (2×1) reconstruction of Si(001) therefore make it easier for the stress induced in the removal process to be transmitted along rather than between dimer rows.

The above mechanism for the anisotropy of the removal process observed on Si(001) suggests that substrates or ultrathin films that have an anisotropic surface structure consisting of well-separated groupings of atoms should be good candidates for patterning into atomic-scale wire structures having atomically straight edges. For example, monolayers of germanium, silver, or tin

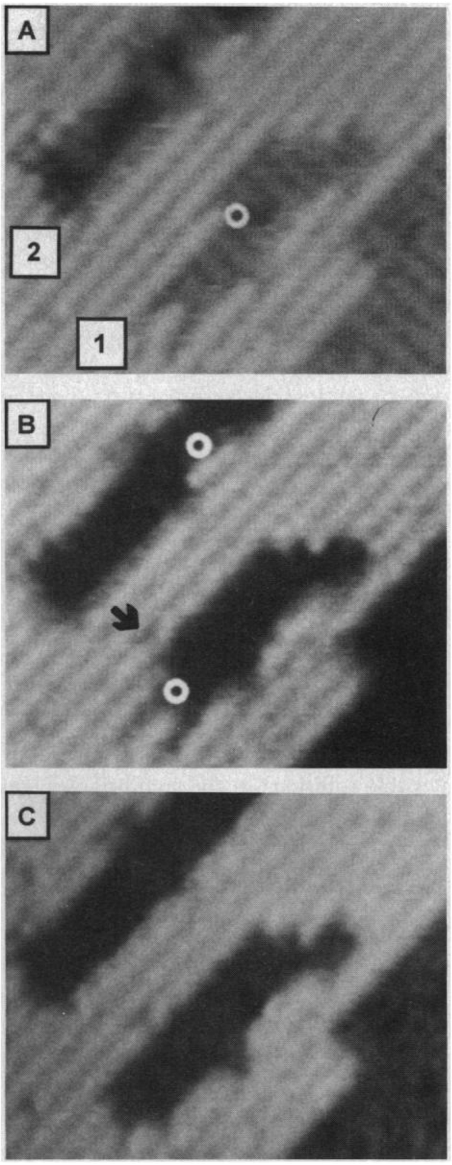

Fig. 6. Rough trenches trimmed by using threshold voltage pulses (−3.6 V) to remove dimer row segments and define a ridge 23 Å wide having atomically straight edges. (**A**) Trenches 1 and 2, discussed in Fig. 4 (a dimer row segment has been removed from trench 1). The open circles indicate the tip position where the next removal attempt would be made. (**B**) A segment six dimers long has been removed at the desired location from trench 1. (**C**) The final structure is created by additionally removing a segment six dimers long from trench 2, a segment six dimers long from the upper edge of trench 1, and an adjacent segment three dimers long from the center of trench 1. All images are ~(200 Å by 200 Å). The arrow in (B) points to the only defect (unintended removal) that occurred in the total sequence of removal attempts.

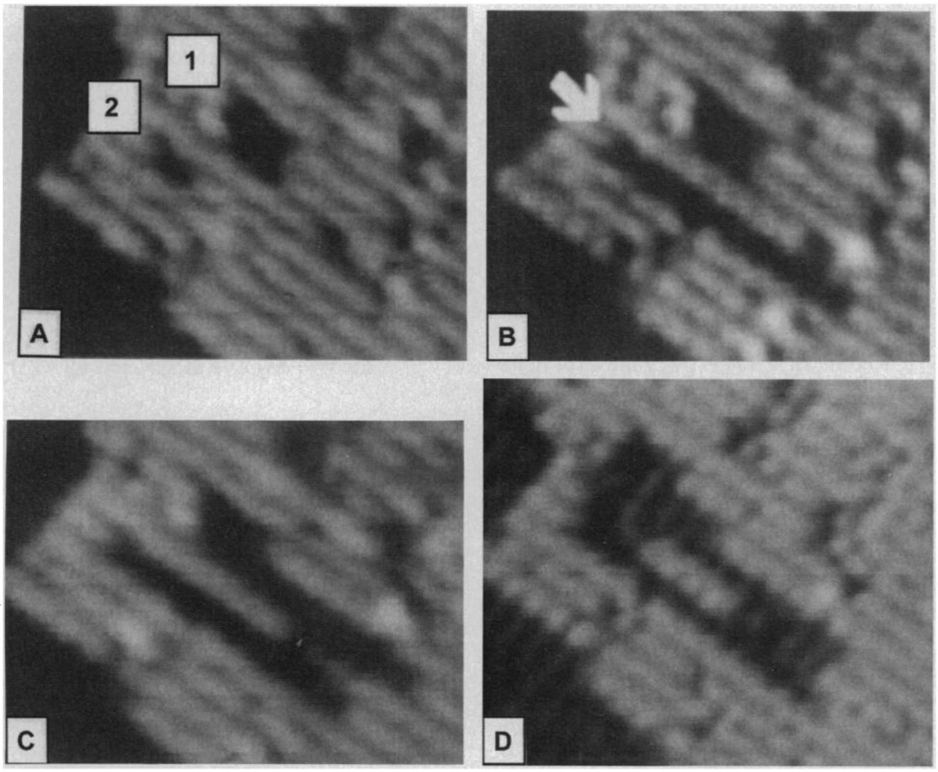

Fig. 5. Fabrication of an island one dimer wide on Si(001). (**A**) Two pits fabricated using threshold voltages at $s = 1.5$ Å (pit 1) and $s = 1.1 \pm 0.3$ Å (pit 2). (**B**) A trench one dimer wide and nineteen dimers (77 Å) long that was fabricated by repeatedly removing atoms from an individual dimer row, starting at the lower right end of pit 2. (**C**) Situation after forming another single-dimer-wide trench starting from the bottom row of pit 1. (**D**) Fabricated island that is one dimer wide and five dimers long, isolated by a moat one atomic layer deep. All images are ~(130 Å by 100 Å).

on Si(001) should be good candidates because they have a dimer row structure.

At room temperature, the small structures we have made are stable for as long as we have observed them (several hours). We can roughly estimate their thermal stability from available values of the activation energies for desorption of dimers from S_A (*17, 18*) and S_B steps (*17–19*). Bridges that have only S_A edges (Fig. 6) decompose most easily by removal of a dimer from an S_A edge. The theoretical value of the energy required for this process is ~2.1 eV (*17*). If we use an Arrhenius relation with an attempt frequency of 10^{13} s^{-1}, the predicted decay rate at room temperature is one defect created in ~10^{10} years. However, the time to create one defect becomes only ~1 min at 325°C, a moderate temperature by the standard of present semiconductor processing. For the island structure (Fig. 5), the easiest decomposition mechanism is the removal of dimers from the ends of rows. Experimental (*19*) and theoretical (*18*) investigations yield an estimate of 1.4 to 1.7 eV for the energy to remove a dimer from an S_B edge. If we use 1.5 eV as a mean value, the average time to create one defect is ~100 years at room temperature and ~10 ms at 325°C. These estimates indicate that the issue of structural integrity will play an important role in any potential technological use of atomic-scale silicon structures. Possible solutions to the stability problem include inducing chemical stabilization, burying the structures, or processing at lower temperatures than those used today.

REFERENCES AND NOTES

1. J. A. Stroscio and D. M. Eigler, *Science* **254**, 1319 (1991).
2. S. Hosoki, S. Hosaka, T. Hasegawa, *Appl. Surf. Sci.* **60/61**, 643 (1992).
3. M. Aono, A. Kobayashi, F. Grey, H. Uchida, D. Huang, *Jpn. J. Appl. Phys.* **32**, 1470 (1993).
4. M. F. Crommie, C. P. Lutz, D. M. Eigler, *Science* **262**, 218 (1993).
5. D. M. Eigler, C. P. Lutz, W. E. Rudge, *Nature* **352**, 600 (1991).
6. R. S. Becker, J. A. Golovchenko, B. S. Swartzentruber, *ibid.* **325**, 419 (1987).
7. H. J. Mamin, S. Chiang, H. Birk, P. H. Guethner, D. Rugar, *J. Vac. Sci. Technol. B* **9**, 1398 (1991).
8. R. M. Silver, E. E. Ehrichs, A. L. de Lozanne, *Appl. Phys. Lett.* **51**, 247 (1987).
9. W. Li, J. A. Virtanen, R. M. Penner, *ibid.* **60**, 1181 (1992).
10. M. A. McCord and R. F. W. Pease, *J. Vac. Sci. Technol. B* **5**, 430 (1987).
11. J. A. Dagata *et al.*, *Appl. Phys. Lett.* **56**, 2001 (1990).
12. I.-W. Lyo and Ph. Avouris, *Science* **253**, 173 (1991).
13. A. Kobayashi, F. Grey, R. S. Williams, M. Aono, *ibid.* **259**, 1724 (1993).
14. Y. Hasegawa and Ph. Avouris, *ibid.* **258**, 1763 (1992).
15. B. S. Swartzentruber, Y.-W. Mo, M. B. Webb, M. G. Lagally, *J. Vac. Sci. Technol. A* **7**, 2901 (1989).
16. B. S. Swartzentruber, Y.-W. Mo, R. Kariotis, M. G. Lagally, M. B. Webb, *Phys. Rev. Lett.* **65**, 1913 (1990).
17. Z. Y. Zhang, H. Chen, B. C. Bolding, M. G. Lagally, *ibid.* **71**, 3677 (1993).
18. Z. Y. Zhang, unpublished results.
19. N. Kitamura, B. S. Swartzentruber, M. G. Lagally, M. B. Webb, *Phys. Rev. B* **48**, 5704 (1993).
20. This research was supported by NSF grant DMR 93-04912 and by the Air Force Office of Scientific Research. We thank J. Vasek and F. Wu for help with the experiments and P. Avouris, N. Kitamura, and Z. Y. Zhang for useful discussions.

25 March 1994; accepted 6 June 1994

Fluctuations and Supercoiling of DNA

John F. Marko* and Eric D. Siggia

Frequently, DNA in vivo is organized into loops that are partially underwound and consequently form interwound helical supercoils. Methods from polymer statistical mechanics are used to show how the competition between entropy (thermal fluctuations) and elastic energy determines supercoil radius and pitch, in good agreement with recent experiments and simulations. Supercoil reorganization by means of slithering (reptation) of the DNA along the supercoil is argued to be a slow process. Extension of supercoiled DNA by an applied force shows a number of unexpected features, including coexistence of interwound and helical states.

Closed loops of double-stranded DNA are ubiquitous in organisms ranging from certain viruses and prokaryotes, in which the entire genome (or accompanying plasmids) is a single loop, to eukaryotes, in which chromosomes are organized by DNA-binding proteins into 50- to 100-kb loops (*1–3*). These loops change conformation subject to topological constraints, such as the double-helix linking number *Lk* (*4, 5*), which is conserved as long as the strands remain unbroken. The conformational biases induced by the *Lk* constraint are manifest in the writhing or supercoiling of the molecule, analogous to the familiar buckling of a twisted tube or wire. Supercoiling is believed to play a biological role in that elaborate cellular machinery has evolved to manipulate *Lk* either by direct enzymatic action or more indirectly by binding to particular proteins (*1*).

Conventionally, linking number perturbations of a loop of length L are reported with a fractional linking number $\sigma = Lk/Lk_0 - 1$, where $Lk_0 = L/h$ is the number of helix repeats along an open chain of length L; for B-form DNA, $h = 3.4$ nm (*1*). Except in thermophilic bacteria, σ is negative and approximately equal to -0.05. Further unwinding of the double helix to $\sigma < -0.10$ unbinds the strands.

The many studies of elastic equilibria (*6*) of loops with $\sigma \neq 0$ are of limited relevance to the situations encountered biologically because DNA loops are typically much longer than the thermal persistence lengths, which are on the order of 50 nm. Arduous Monte Carlo computer simulations (*7*) have correctly accounted for thermal fluctuations and have achieved impressive agreement with experiment (*8*), except in cases where cation-induced condensation may play a role (*9*). In this report, we reproduce the results of two previous reports (*7, 8*) semiquantitatively by simple statistical-mechanical calculations that provide useful insight into how entropy and elastic energy compete to determine the observed supercoil structure. In addition, several experimentally testable predictions are made.

The energy (enthalpy) of deformation of the double helix (*5*) depends on its local curvature $\kappa(s)$ and local excess twist $\Omega(s)$, both of which have units of inverse length and depend on s, the arc length along the axis of the molecule. The energy per unit length in units of k_BT (where k_B is Boltzmann's constant and T is temperature) is $\epsilon = \frac{1}{2}(A\kappa^2 + C\Omega^2)$ (*10*), where $A \approx 50$ nm and $C \approx 75$ nm are the persistence lengths for bends and twists, respectively (*11*). The total molecular twist (*2, 3*) is

$$Tw = \int_0^L ds[\omega_0 + \Omega(s)]/2\pi \qquad (1)$$

where $\omega_0 = 2\pi/h = 1.85$ nm^{-1} is the local twist of an undistorted molecule. The values of Tw and Lk are related by $Lk = Tw + Wr$, where Wr is the "writhe" of the molecule (*4, 5*), a quantity independent of $\Omega(s)$.

The probability distribution of conformations is given by the Boltzmann distribution $\exp[-\int ds\,\epsilon(s)]$. The Ω dependence can be explicitly averaged out and reexpressed with the constraint $Tw = Lk - Wr$. However, the remaining average over backbone conformation is complex and has only been implemented numerically (*7, 12*).

For small $|\sigma|$, perturbation theory around a free untwisted chain is reasonable, provided that the number of added links per twist persistence length, $\chi = C\omega_0|\sigma| \approx 130|\sigma|$, is less than about unity. The excess free energy

---

Laboratory for Atomic and Solid State Physics, Clark Hall, Cornell University, Ithaca, NY 14853–2501, USA.

*Present address: Center for Theoretical Studies in Physics and Biology, The Rockefeller University, 1230 York Avenue, New York, NY 10021–6399, USA.